Nanosecond-precision Time-of-Arrival Estimation for Aircraft Signals with low-cost SDR Receivers

Roberto Calvo-Palomino
IMDEA Networks Institute, Spain
University Carlos III of Madrid
roberto.calvo@imdea.org

Fabio Ricciato
University of Ljubljana, Slovenia
fabio.ricciato@fri.uni-lj.si

Blaz Repas
University of Ljubljana, Slovenia
br9404@student.uni-lj.si

Domenico Giustiniano
IMDEA Networks Institute, Spain
domenico.giustiniano@imdea.org

Vincent Lenders
armasuisse, Switzerland
vincent.lenders@armasuisse.ch

arXiv:1802.07016v1 [eess.SP] 20 Feb 2018

ABSTRACT

Precise Time-of-Arrival (TOA) estimations of aircraft and drone signals are important for a wide set of applications including aircraft/drone tracking, air traffic data verification, or self-localization. Our focus in this work is on TOA estimation methods that can run on low-cost software-defined radio (SDR) receivers, as widely deployed in Mode S / ADS-B crowdsourced sensor networks such as the OpenSky Network. We evaluate experimentally classical TOA estimation methods which are based on a cross-correlation with a reconstructed message template and find that these methods are not optimal for such signals. We propose two alternative methods that provide superior results for real-world Mode S / ADS-B signals captured with low-cost SDR receivers. The best method achieves a standard deviation error of 1.5 ns.

1 INTRODUCTION

Aircraft and unmanned aerial vehicles continuously transmit wireless signals for air traffic control and collision avoidance purposes. These signals are either sent as responses to interrogations by secondary surveillance radars (SSR) or automatically on a periodic basis (ADS-B). Both types of signals are transmitted over the so-called *Mode S* data link [12] on the 1090 MHz radio frequency.

Over the last few years, sensor network projects have emerged which collect those signals using a crowd of low-cost software-defined radio (SDR) receivers such as e.g. the OpenSky Network [20], Flightaware [5], Flightradar24 [6] and many others. These sensor networks can leverage the time-of-arrival (TOA) of Mode S signals for various kinds of applications, including aircraft localization [20, 22], air traffic data verification [13, 16, 17, 19, 21], and self-localization [15]. In those applications, a set of cooperating receivers measure *locally* the TOA of the arriving signals and then send these data to a central computation server. By joint processing the TOA of the same signal arriving at different receivers, the central server is able to estimate the location of the transmitter, the location of the receivers, or the exact time when the signal was transmitted.

The accuracy of these applications heavily depends on the precision of the TOA estimation, and in order to estimate positions up to a few meters it is necessary to estimate the TOA with nanosecond precision. The goal of this work is to provide a method for the TOA estimation of Mode S signals that delivers nanosecond-level precision even with low-cost SDR receivers, such as the widespread RTL-SDR dongle [3]. We show that existing TOA estimation approaches based on a cross-correlation with a reconstructed signal template are sub-optimal in the particular context of Mode S signals. In fact, the loose tolerance margins allowed by the specifications on the shape and position of each individual symbol within the packet (up to ± 50 ns) adds uncertainty to the reconstruction of the whole packet waveform at the receiver.

We propose two alternative methods that improve the precision and at the same time reduce the computational load.We test different variants of TOA estimation on real-world signal traces captured with RTL-SDR, which is currently the cheapest SDR device on the market and widely used by crowdsourced sensor networks. Our results show that the best proposed method delivers TOA estimates with a standard deviation error of 1.5 ns. We further identify the limited dynamic range of the RTL-SDR device (less than 50 dB with 8-bit analog-to-digital converter (ADC) and fixed automatic-gain controller (AGC)) as the main performance bottleneck, and show that sub-nanosecond precision is achievable for signals that are not clipped due the limited dynamic range of the device.

2 BACKGROUND

This section provides background on aircraft signals which we rely on to estimate the TOA, and the limitations of classical TOA estimation methods.

2.1 Mode S signal format

Hereafter we briefly review the physical-layer format of SSR Mode S [18] reply and ADS-B messages transmitted by aircrafts on the 1090 MHz channel. Both packet formats consist of a preamble of 8 μs plus a payload of 112 or 56 bits (only for other SSR Mode S replies) sent at 1 Mbps rate, for a total duration of 120 μs or 64 μs, respectively. The information bits are modulated with a simple Binary Pulse Position Modulation (BPPM) scheme as illustrated in Fig. 1: the symbol period of 1 μs is divided into two "chips" of 0.5 μs, and the high-to-low and low-to-high transitions encode bits "1" and "0", respectively. It is clear from Fig. 1 that the BPPM modulation produces two types of pulses of different duration, denoted hereafter as "Type-I" and "Type-II". Type-I pulses have a nominal duration of one chip period and are produced by the bit sequences "00", "11" and "10". The preamble consists of four Type-I pulses. On the other hand, Type-II pulses have a nominal duration of two chip periods and are produced exclusively by the "01" sequence.

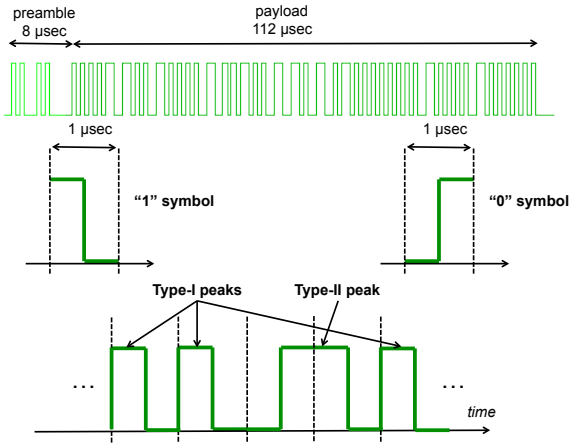


Figure 1: Mode S packet structure with a binary PPM modulation.

On average, we expect approximately $112/2 = 56$ Type-I and $112/4 = 28$ Type-II pulses for a payload of 112 bits.

The real-valued baseband signal is then modulated on the 1090 MHz carrier frequency and transmitted over the air. On the receiver side, the decoding process relies exclusively on the signal *amplitude*, since in BPPM the signal *phase* carries no information.

2.2 Limitation of standard TOA methods

The standard "course book" approach to TOA estimation in the Additive White Gaussian Noise (AWGN) channel is a correlation filter [14]: the received signal is cross-correlated with a known template corresponding to the source signal, and the point in time maximizing the cross-correlation module is taken as TOA estimate.

The correlation method relies on the assumption that *the source signal can be reconstructed very precisely* at the receiver, based on the signal specifications and knowledge of the payload bits $\boldsymbol{p}_m$. Under this assumption, the correlation method represents the Maximum Likelihood Estimator (MLE) [14]. However, this assumption is problematic in the particular case of *real-world* Mode S signals. In fact, the standard specifications tolerate up to ±50 ns jitter in the *position* of each individual pulse within the packet: such high tolerance value is practically negligible for the decoding process, but not for the task of determining the TOA with nanosecond precision. As to the *shape* of each pulse, tolerance values of 50 ns are allowed for the pulse *duration* and *rise time* and up to 150 ns for the *decay time*, while pulse amplitude may vary up to 2 dB (approximately 60%). Such loose tolerance margins introduce uncertainty in the prediction of the shape and position of the pulses in the source signal. Considering that Mode S signals are typically received with high SNR, such an uncertainty might well prevail over the effect of additive noise. Consequently, the correlation-based approach with a known packet template is no longer guaranteed to be optimal, motivating the quest for alternative, more precise methods.

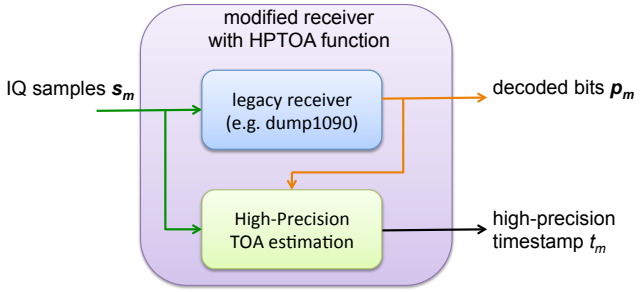


Figure 2: Block diagram of improved receiver with high-precision TOA estimation.

3 OUR TOA ESTIMATION METHODS

In this section we describe the general approach to TOA estimation based on the decoded payload and received signal samples, and then present the different TOA estimation algorithms that were tested.

3.1 Signal acquisition architecture

In the software domain, the high-precision TOA estimation process can be seen as an additional function that is optionally called within the receiver and remains independent from the main decoding process. As such, it can be implemented on top of any legacy receiver, including but not limited to the widely adopted open-source tool `dump1090` [1]. The overall block diagram of the proposed scheme is exemplified in Fig. 2. The legacy receiver takes as input a stream of complex in-phase and quadrature (IQ) samples collected at sampling rate f_s (for RTL-SDR hardware $f_s = 2.4$ MHz). The legacy receiver seeks to detect and decode the incoming packet and, if successful, provides as output the decoded bit sequence $\boldsymbol{p}_m$ along with the indication of the leading IQ sample of the detected packet.

Denote by $\boldsymbol{s}_m$ the sequence of complex IQ samples corresponding to the whole packet. The sequence includes approximately 300 samples since we also pick a few samples immediately before and after the packet in order to mitigate edge effects. The sample vector $\boldsymbol{s}_m$ and the decoded bit vector $\boldsymbol{p}_m$ represent the input to our TOA estimation block.

3.2 Proposed methods: *CorrPulse* and *PeakPulse*

Hereafter we describe two novel TOA estimation algorithms specifically developed for Mode S signals. For a generic packet m we shall denote by K_m the total number of pulses in the whole packet (preamble and payload). The input vector of complex samples $\boldsymbol{s}_m$ is preliminarily upsampled by a factor N and transformed into vector $\boldsymbol{s}'_m$ (for a review of upsampling process see e.g. [10]). To illustrate, Fig. 3 plots an excerpt of the amplitude of both vectors, namely $|\boldsymbol{s}_m|$ (top plot) and $|\boldsymbol{s}'_m|$ (bottom plot), for a generic packet found in a real-world trace.

The key aspect of the proposed algorithms is that the actual temporal position $\hat{\tau}_k$ of the generic kth pulse within the packet is estimated *independently* from other pulses, with no need to reconstruct a template for the whole packet. For each pulse $k \geq 2$,

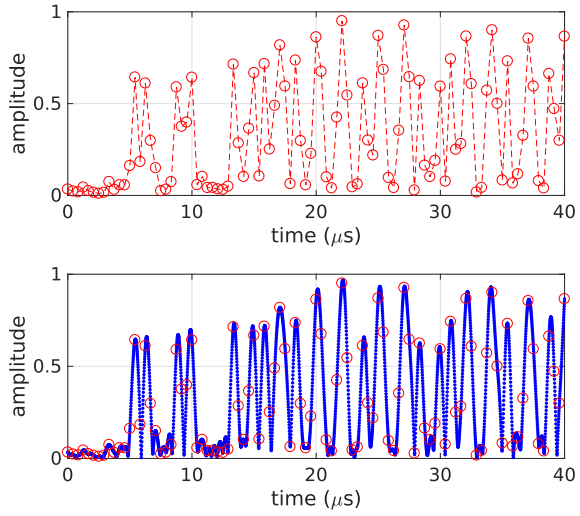


Figure 3: Example of received signal amplitude corresponding to the preamble and initial payload of a real ADS-B packet. Original samples at $f_s = 2.4$ MHz (top, red circles) and corresponding upsampled version (bottom, blue line).

we compute the individual shift $\Delta\tau_k \stackrel{\text{def}}{=} \hat{\tau}_k - \tau_k$, i.e., the difference between the estimated and nominal pulse position relative to the (estimated) position of the first pulse. Finally, the pulse shifts are averaged in order to obtain the final TOA estimate:

$$\hat{t} = \hat{\tau}_1 + \frac{1}{K_m - 1} \sum_{k=2}^{K_m} \Delta\tau_k \tag{1}$$

The two proposed variants differ in the way individual pulse position estimates are obtained, and which type(s) of pulses are considered. In the first variant, labeled *CorrPulse*, each pulse position is determined through pulse-level cross-correlation of the upsampled vector s'_m with the corresponding nominal pulse shape. Both Type-I and Type-II pulses are considered in the final averaging.

In the second variant, labeled *PeakPulse*, individual pulse positions are determined by simply picking the local maximum point value within the pulse interval, with no cross-correlation operation. In this variant only Type-I pulses are considered, while Type-II pulses are ignored. This is motivated by the fact that Type-II pulses have lower curvature, hence their local peaks cannot be identified as reliably as for Type-I pulses.

4 EVALUATION METHODOLOGY

This section describes how we evaluate our new methods. First, we introduce the other competing methods taken as reference for the comparison. Then, we present the testbed setup with commercial low-cost hardware. Finally, we provide details on the procedure adopted to empirically assess the precision of the TOA measurement methods in the given setup.

4.1 Other methods for comparison

4.1.1 Correlation with whole-packet template: CorrPacket. This is the canonical cross-correlation method with a known signal template.

For every packet m, the whole packet template is reconstructed from the decoded bits $\boldsymbol{p}_m$ and then cross-correlated with the amplitude of the incoming signal. Here also, upsampling by a factor N is adopted to achieve sub-sample precision. Within the template, the kth pulse is positioned at the nominal time τ_k. As to the pulse shapes, we have tested two different variants: "Rectangular" (R), and "Smoothed" (S). The two versions will be denoted by *CorrPacket/R* and *CorrPacket/S*. The rectangular pulses have a nominal duration of 0.5 μs and 1 μs for Type-I and Type-II pulses, respectively, and zero rise/decay times. The rectangular pulse mask is represented exclusively by "0" and "1" values, hence multiplications with another vector reduce to element selection, which saves on computation load. The "Smoothed" shape corresponds to the output of a low-pass filter with passband of 2.4 MHz—matched to the bandwidth of the RTL-SDR receiver—when the input signal is a nominal Type-I/Type-II pulse with the minimum decay/rise time of 50 ns as per specifications [11].

4.1.2 Existing dump1090 based implementations. We also evaluate the precision of the timestamp reported by the mutability fork of the open-source tool `dump1090` [1]. Furthermore, we test on our traces also the method adopted by Eichelberger et al. in a recent ACM SenSys'17 paper [15] which is also based on dump1090. Code inspection revealed that this method is based on a cross-correlation (implemented in frequency domain) with a partial packet template consisting of the preamble plus one quarter of the payload, with rectangular pulses and upsampling factor $N = 25$.

4.2 Testbed setup

The experimental setup consists of two identical sensors connected to a single antenna through a power splitter and cables of identical length. The sensors are located on the roof of a building as Figure 4 shows. Every sensor consists of one RTL-SDRv3 "Silver" model [4] attached to a Raspberry Pi-3 [2]. The AGC gain is set to a fixed value, manually tuned to maximize the packet decoding rate. The sampling rate was set to $f_s = 2.4$ MHz, the maximum value that our setup is able to acquire with sample losses. Every I and Q sample is represented with 8 bit. The full stream of IQ samples are recorded one and processed multiple times offline. Our results are based on a sample trace of 5 minutes collected in Thun (Switzerland) on 02-Aug-2017 at time 09:41. The number of ADS-B packets that are correctly decoded *at both sensors* by the `dump1090` open-source tool [1] amount to 26445 from 59 different aircraft.

4.3 Evaluation Metrics

In this section, we briefly describe the methodology adopted to assess the precision of the different TOA estimation methods. The problem is not trivial, since our receivers are not synchronized and the "true" TOA is unknown. Therefore, we developed an evaluation method which allows us to quantify the TOA precision without a ground truth. Denote by $t_{m,i}$ the *true* absolute arrival time of packet m to receiver i and by $\hat{t}_{m,i}$ the corresponding *measured* TOA

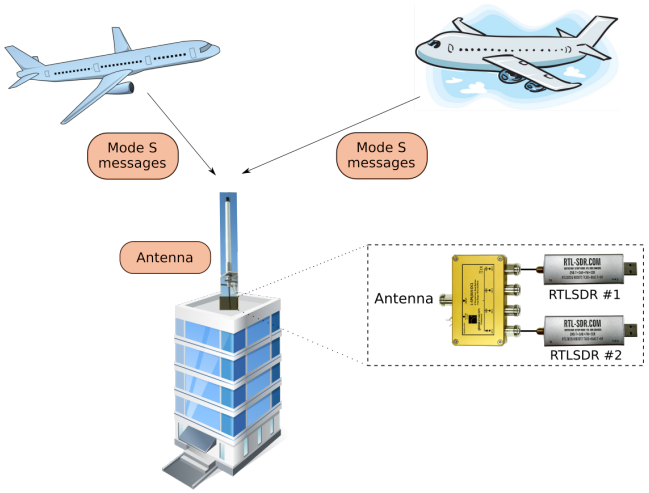


Figure 4: Experimental setup. Two identical receivers connected to the same antenna via a splitter are collecting Mode S messages sent by aircraft.

(by the method under test). In general, the measured value $\hat{t}_{m,i}$ is affected by two distinct sources of error, namely clock error and measurement noise:

$$\hat{t}_{m,i} = t_{m,i} + \xi_i(t)|_{t=t_{m,i}} + \epsilon_{m,i}. \tag{2}$$

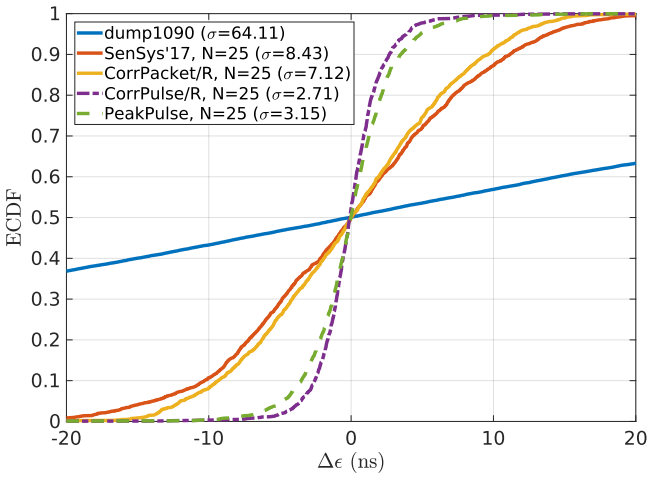
The term $\xi_i(t)$ models the *clock error* between the receiver clock and the absolute time reference, and can be modeled by a *slowly-varying* function of time. Its magnitude depends on the *hardware* characteristics of the device, and specifically on the stability of the local oscillator.

The term $\epsilon_{m,i}$ represents the measurement noise in the TOA estimation process and is modeled by a *random variable* with zero mean and variance σ^2_{TOA}. The *precision* of the TOA estimate, defined as the reciprocal of the noise variance, is *independent* of the clock error. The goal of the present study is to reduce σ^2_{TOA}. The problem of counteracting the clock error component remains outside the scope of the present contribution. Here it suffices to mention that the clock error can be mitigated by adopting receivers with GPS Disciplined Oscillators (GPSDO), or it can be estimated and compensated in post-processing [7–9].

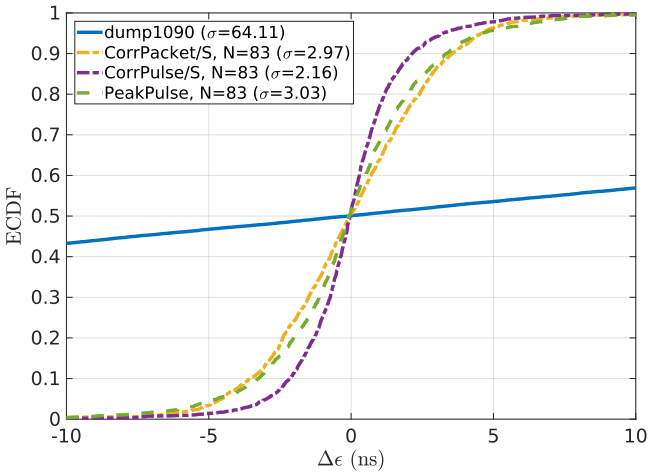
Hereafter we illustrate the methodology to experimentally quantify the empirical TOA standard deviation $\hat{\sigma}_{\text{TOA}}$ notwithstanding the presence of a non-zero clock error component. First, we need to get rid of the unknown *true* absolute arrival time $t_{m,i}$ in Equation (2). Since we use two identical receivers attached to the same antenna, we can set $t_{m,1} = t_{m,2} = t_m$ and subtract the TOA measurements at the two sensors to obtain the corresponding time difference:

$$\hat{\Delta t}_m \stackrel{\text{def}}{=} \hat{t}_{m,2} - \hat{t}_{m,1} = \Delta\xi(t_m) + \Delta\epsilon_m \tag{3}$$

wherein $\Delta\xi(t) \stackrel{\text{def}}{=} \xi_2(t) - \xi_1(t)$ denotes the compound clock error, and $\Delta\epsilon_m \stackrel{\text{def}}{=} \epsilon_{m,2} - \epsilon_{m,1}$ the compound measurement error with variance $\sigma^2_{\Delta\epsilon} = 2\sigma^2_{\text{TOA}}$. At short time-scales, within the coherence time of the process $\Delta\xi(t)$, the clock error represents a systematic



(a) Low upsampling factor



(b) High upsampling factor

Figure 5: ECDF of $\Delta\epsilon$ residuals.

error, i.e. a *bias* term that can be estimated and removed in order to estimate the error *variance* $\sigma^2_{\Delta\epsilon}$. We do so by modeling the slowly-varying function $\Delta\xi_i(t)$ by a polynomial whose coefficients are estimated by standard order-recursive Least Squares (refer to [14, Chapter 8] for details). After removing the estimated clock error component, we obtain a set of residuals $\{\Delta\epsilon\}$. Their Mean Square Error (MSE) represents an empirical estimate of twice the TOA variance $MSE_{\Delta\epsilon} = 2 \cdot \sigma^2_{\text{TOA}}$. Accordingly, their Root Mean Square Error (RMSE) provides a direct empirical estimate of the TOA error standard deviation, formally:

$$\hat{\sigma}_{\text{TOA}} = \frac{1}{\sqrt{2}} RMSE_{\Delta\epsilon} \approx 0.7 \cdot RMSE_{\Delta\epsilon}.$$

5 NUMERICAL RESULTS

We now present the results on the precision of the different TOA estimation methods as evaluated in our testbed.

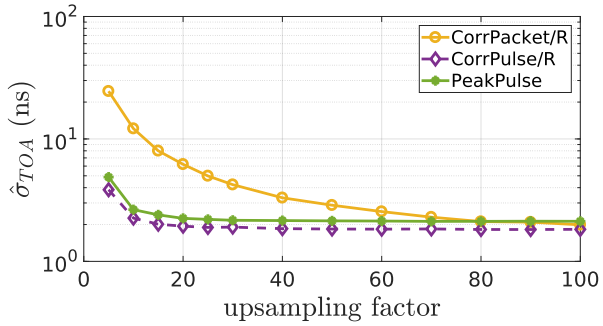


Figure 6: TOA standard dev. error vs. upsampling factor N

5.1 Error distribution

In Fig. 5 we plot the Empirical Cumulative Distribution Function (ECDF) of the residuals $\Delta\epsilon$'s obtained with different TOA estimation methods for all the packets in the test trace. The corresponding values of the TOA error standard deviation $\hat{\sigma}_{\text{TOA}}$ are reported in the leftmost column of Table 1.

For those applications where the computation load is of concern, it is relevant to investigate the performance of the different methods with moderate value of the upsampling factor ($N = 25$). For *CorrPacket* and *CorrPulse*, we consider the rectangular pulse shape with binary 0/1 values, due to lower computation load. Referring to Fig. 5(a), we observe that the proposed *PeakPulse* algorithm achieves a $RMSE_{\Delta\epsilon} = 3.15$ ns, less than half the value of the canonical *CorrPacket/R* method. It is remarkable that such good result was obtained with no cross-correlation operation. Fig. 6 shows $\hat{\sigma}_{\text{TOA}}$ for different values of the upsampling factor N. We observe that the precision of the proposed methods *PeakPulse* and *CorrPulse/R* improves faster than *CorrPacket/R* with increasing N. These results indicate that *PeakPulse* should be preferred when computation load is at premium.

Next we consider applications that enjoy abundant computation power, for which the main goal is to maximize precision and computation load is not of concern. For these, it is convenient to consider higher upsampling factors ($N = 83$ in our case) and, for the cross-correlation methods, the more elaborated "Smoothed" pulse shape. The latter matches more closely the pulse shape passed through the RTL-SDR front-end, leading to slightly higher precision than the simpler "Rectangular" shape, as can be verified from Table 1. The ECDF of the residuals $\Delta\epsilon$'s for these methods are plotted in Fig. 5(b). It can be seen that the proposed *CorrPulse/S* method is more precise than the classical *CorrPacket/S* method, and achieves $RMSE_{\Delta\epsilon} = 2.16$ ns corresponding to $\hat{\sigma}_{\text{TOA}} = 1.51$ ns.

5.2 Error vs. signal strength

In the following, we investigate the impact of signal strength on the TOA error obtained with the most precise method, namely *CorrPulse/S with* $N = 83$. For a generic packet m and sensor i, we denote by $\gamma_{m,i}$ the average of the squared pulse height over all pulses — an indicator of the arriving packet strength. Furthermore, we denote by $\beta_{m,i}$ the number of pulses that are clipped in the receiver due to one or more of the corresponding IQ samples saturating the ADC.

estimation method	$\hat{\sigma}_{\text{TOA}}$ [nanoseconds]			
	all packets	L	M	H
legacy dump1090	45.20	44.94	45.19	45.43
SenSys'17, $N = 25$	5.90	6.11	5.88	5.78
CorrPacket/R, $N = 25$	4.98	5.48	4.85	4.94
CorrPacket/R, $N = 83$	2.14	3.04	1.78	2.35
CorrPacket/S, $N = 83$	2.07	3.00	1.68	2.275
CorrPulse/R, $N = 25$	1.89	2.75	1.56	1.86
CorrPulse/R, $N = 83$	1.63	2.72	1.04	1.77
CorrPulse/S, $N = 83$	1.51	2.60	0.79	1.77
PeakPulse, $N = 25$	2.20	3.36	1.70	2.23
PeakPulse, $N = 83$	2.12	3.44	1.62	2.17

Table 1: Empirical estimates of TOA error standard deviation $\hat{\sigma}_{\text{TOA}}$.

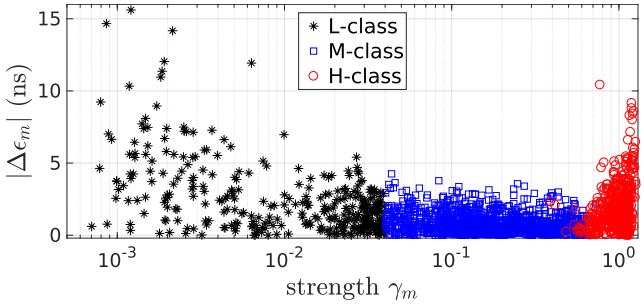


Figure 7: Absolute error $|\Delta\epsilon_m|$ vs. packet strength γ_m.

In Fig. 7, we plot for each individual packet m the absolute value of the residual error $|\Delta\epsilon_m|$ obtained with *CorrPulse/S* ($N = 83$) against the mean signal strength between the two sensors $\gamma_m \stackrel{\text{def}}{=} \frac{\gamma_{m,1}+\gamma_{m,2}}{2}$. Each packet is classified into one of three classes: packets with $\gamma_m \leq 0.04$ are labeled by "L", packets with $\min_{i=1,2} \beta_{m,i} \geq 10$ are labeled with "H", and all remaining packets are labeled with "M". The three classes are marked respectively with black, red and blue markers in Fig. 7. The estimated TOA error standard deviation obtained by each method for each class are reported in Table 1. On one extreme, timing estimates for "L" packets with lower strength are impaired by quantization noise. On the other extreme, packets received with high strength are subject to ADC clipping, a form of distortion that clearly degrades timing precision. As expected, these two classes yield higher error with all methods. Between the two extremes, the strength of "M" packets fits well the dynamic range: for these, the proposed method achieves $\hat{\sigma}_{\text{TOA}} = 0.79$ ns.

In our traces, less than 60% of all packets fall into class "M". With better hardware, and specifically with more ADC bits and larger dynamic range, it would be possible to tune the AGC gain so as to increase the fraction of packets falling in this class, thus improving the overall precision.

The above results indicate that the received packet metrics $\gamma_{m,1}$ and $\beta_{m,i}$ can be used to provide, *for each individual TOA measurement* $\hat{t}_{m,i}$, also an indication of the expected precision, i.e., of

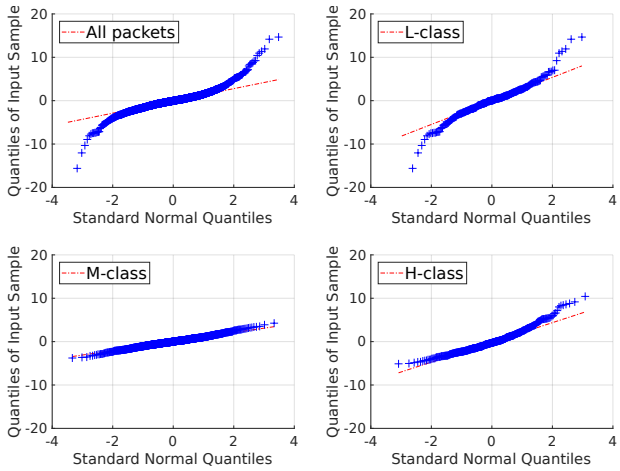


Figure 8: Quantile-quantile plot of empirical errors $\Delta\epsilon$ vs. normal distribution.

the error variance $\hat{\sigma}^2_{m,i}$ affecting each individual measurement. In this way, algorithms that take TOA measurements as input (e.g., for position estimation) have the possibility to *weight* optimally each individual input measurement, as done e.g. in Weighted Least Squares methods [23].

Finally, we find that *within each class* the empirical error distribution is very well approximated by the Gaussian distribution, as seen from the normal Q-Q plots in Fig. 8. This justifies the adoption of Least Squares (LS) methods for position estimation problems based on input TOA measurements [7], since for normally distributed input errors the LS solution coincides with the Maximum Likelihood estimate.

6 CONCLUSIONS AND OUTLOOK

We have presented two variants of a novel TOA estimation method for Mode S signals that does not rely on long cross-correlations with the template of a full packet. The most precise variant, namely *CorrPulse/S*, involves only short cross-correlation operations on individual pulses. The other variant, namely *PeakPulse*, is lighter to compute, involves no cross-correlation operation and works well also with moderate upsampling factors.

We have shown that such algorithms can achieve TOA estimates with nanosecond-level precision even with real-world signals captured with the cheapest SDR hardware that is currently available, namely RTL-SDR. A closer look at the test results reveals that the main limiting factor for the achievable TOA precision with RTL-SDR is the limited dynamic range — less than 50 dB with 8-bit ADC and fixed AGC — resulting in a large fraction of packets being clipped or drowned into quantization noise. For packets that are received with signal strength well within the dynamic range of the receiver, the *CorrPulse/S* achieves sub-nanosecond precision. It can be expected that precision can be further improved with better hardware. The *PeakPulse* method has been implemented in C, integrated in the dump1090 receiver and is released as open-source[1].

[1] http://github.com/openskynetwork/dump1090-hptoa

ACKNOWLEDGMENTS

This work has been funded in part by the Madrid Regional Government through the TIGRE5-CM program (S2013/ICE-2919). We would like to thank Manuel Eichelberger from ETH Zurich for sharing the code we used in our evaluation for comparison purposes.

REFERENCES

[1] 2016. dump1090, https://github.com/mutability/dump1090. https://github.com/mutability/dump1090.
[2] 2016. Raspberry Pi 3 Model B, https://www.raspberrypi.org/products/raspberry-pi-3-model-b/.
[3] 2016. *Silver v3 specifications.* http://www.rtl-sdr.com/buy-rtl-sdr-dvb-t-dongles/.
[4] 2017. RTL-SDR dongle v3, http://www.rtl-sdr.com/buy-rtl-sdr-dvb-t-dongles/.
[5] 2018. *FlightAware.* http://www.flightaware.com/.
[6] 2018. *FlightRadar24.* https://www.flightradar24.com/.
[7] F. Ricciato, S. Sciancalepore, F. Gringoli, N. Facchi and G. Boggia. 2018. Position and Velocity Estimation of a Non-cooperative Source From Asynchronous Packet Arrival Time Measurements. *IEEE Trans. on Mobile Computing* (2018).
[8] G. de Miguel, J. Portas, J. Herrero. 2005. Correction of propagation errors in Wide Area Multilateration systems. In *Proc. of 6th European Radar Conference.*
[9] G. Galati, M. Leonardi, I.A. Mantilla-Gaviria and M. Tosti. 2012. Lower bounds of accuracy for enhanced mode-S distributed sensor networks. *IET Radar, Sonar and Navigation* (2012).
[10] Fred J. Harris. 2004. *Multirate Signal Processing for Communication Systems.* Prentice Hall.
[11] ICAO. 2007. Aeronautical Communications, Volume IV, Surveillance and Collision Avoidance Systems. (July 2007).
[12] ICAO 2008. *Technical Provisions for Mode S Services and Extended Squitter.* ICAO. Doc 9871, First Edition.
[13] K. Jansen, M. Schäfer, D. Moser, V. Lenders, C. Pöpper, , and J. Schmitt. 2018. Crowd-GPS-Sec: Leveraging Crowdsourcing to Detect and Localize GPS Spoofing Attacks. In *IEEE Symposium on Security and Privacy (S&P).*
[14] S. M. Kay. 1993. *Fundamentals of Statistical Signal Processing, vol. 1, Estimation Theory.* Prentice-Hall.
[15] S. Tanner M. Eichelberger, K. Luchsinger and R. Wattenhofer. 2017. Indoor Localization with Aircraft Signals. In *ACM SenSys.*
[16] V. Lenders M. Strohmeier and I. Martinovic. 2015. Lightweight Location Verification in Air Traffic Surveillance Networks. In *ACM Cyber-Physical System Security Workshop (CPSS).*
[17] D. Moser, P. Leu, V. Lenders, A. Ranganathan, F. Ricciato, and S. Capkun. 2016. Investigation of Multi-device Location Spoofing Attacks on Air Traffic Control and Possible Countermeasures. In *ACM Conference on Mobile Computing and Networking (Mobicom).*
[18] RTCA 2011. *Minimum Operational Performance Standards for Air Traffic Control Radar Beacon System / Mode Select (ATCRBS / Mode S) Airborne Equipment.* RTCA. DO-181E.
[19] M. Schäfer, M. Strohmeier, V. Lenders, and J. Schmitt. 2015. Secure Track Verification. In *Security and Privacy (S&P), 2015 IEEE Symposium on.*
[20] M. Schäfer, M. Strohmeier, I. Martinovic V. Lenders, and M. Wilhelm. 2014. Bringing Up OpenSky: A Large-scale ADS-B Sensor Network for Research. In *13th ACM/IEEE Int. Conf. on Information Processing in Sensor Networks (IPSN'14).*
[21] M. Strohmeier, V. Lenders, and I. Martinovic. 2015. On the Security of the Automatic Dependent Surveillance-Broadcast Protocol. *IEEE Communications Surveys and Tutorials Journal* (2015).
[22] M. Strohmeier, V. Lenders, and I. Martinovic. 2018. A k-NN-based Localization Approach for Crowdsourced Air Traffic Communication Networks. *IEEE Transactions on Aerospace and Electronic Systems (TAES)* (2018).
[23] Tilo Strutz. 2010. *Data fitting and uncertainty: A practical introduction to weighted least squares and beyond.* Vieweg and Teubner.